Plasmon dispersion and dynamic exchange - correlation potentials from two-pair excitations in degenerate plasmas

1996 J. Phys.: Condens. Matter 8 781

(http://iopscience.iop.org/0953-8984/8/7/005)

J. Phys.: Condens. Matter **8** (1996) 781–797. Printed in the UK

Plasmon dispersion and dynamic exchange–correlation potentials from two-pair excitations in degenerate plasmas

H M Böhm†‡, S Conti‡§ and M P Tosi‡§

† Institut für Theoretische Physik, Johannes Kepler Universität, A-4040 Linz, Austria
‡ International Centre for Theoretical Physics, I-34014 Trieste, Italy
§ Istituto Nazionale di Fisica della Materia and Classe di Scienze, Scuola Normale Superiore, I-56126 Pisa, Italy

Received 3 November 1995

Abstract. Electron energy-loss experiments have shown a rapid softening of the bulk plasmon dispersion across the series of the alkali metals. Motivated by these observations, we reconsider the evaluation of the dynamic, long-wavelength exchange–correlation potential $f_{xc}(\omega)$ in the electron fluid, which is of interest for applications in time-dependent density functional theory. The value of $\mathrm{Re}[f_{xc}(\omega_{pl})]$ at the plasma frequency ω_{pl} determines the exchange–correlation contribution to the leading plasmon dispersion coefficient in the homogeneous electron fluid. Whereas an interpolation scheme originally proposed by Gross and Kohn assumes a monotonic increase of $\mathrm{Re}[f_{xc}(\omega) - f_{xc}(0)]$ across the plasma frequency, we examine the possibility of strongly non-monotonic behaviour arising from a resonance process between plasmons and two-pair excitations. This process is evaluated with the help of sum rules and selfconsistency requirements within a single-pole approximation for the dielectric function. The cases of a fermion plasma and of a boson plasma are treated in parallel and the reliability of the results for the fermion plasma at low coupling is tested by calculations within a random-phase approximation for the dielectric function. In all cases it is found that the resonance process accumulates oscillator strength in the neighbourhood of $2\omega_{pl}$, thus decreasing the value of $\mathrm{Re}[f_{xc}(\omega_{pl})]$ below the static value $f_{xc}(0)$ fixed by the compressibility sum rule. Although this lowering does not suffice to account by itself for the measured plasmon dispersion coefficient in the low-density alkali metals, our results provide useful input for combined band-structure and exchange–correlation calculations.

1. Introduction

From electron energy-loss experiments at high resolution vom Felde, Sprösser-Prou and Fink [1] have reported new and accurate data on the plasmon excitation in the alkali metals from Na to Cs. The dispersion relation

$$\omega_k = \omega_{k=0} + \alpha k^2/m + Ck^4 \tag{1.1}$$

($\hbar = 1$) can be fitted to their data up to the critical wave number for the onset of Landau damping. Most interestingly the value of the leading dispersion coefficient α drops rapidly through the series of metals, becoming essentially zero in Rb and negative in Cs. While such behaviour of α with decreasing electron density had been qualitatively predicted already in theories of the homogeneous electron fluid developed since the late sixties [2], the observed decrease is much more pronounced than in the corresponding theoretical results [3–7].

A number of attempts have been made to account for these observations [8–14]. By an *ad hoc* matching of the coupling strength for degenerate electrons onto that of the one-component classical plasma Kalman *et al* [11] claimed that dynamic correlation effects in

0953-8984/96/070781+17$19.50

the homogeneous fluid can account for the observed softening of the plasmon dispersion. Further evidence for this view has come from the work of Lipparini *et al* [13] evaluating the plasmon contribution to the compressibility and f sum rules. In contrast Aryasetiawan and Karlsson [14] have emphasized the role of band-structure effects within a random-phase approximation (RPA) calculation, with special regard to the influence of low-lying d states coming close to the Fermi surface in the heavier alkali metals. It can in fact be expected that both correlation and band-structure effects are relevant for a quantitative account of the observations. This view has been taken by Taut and Sturm [12], who have used local and non-local density functional approaches within existing theories of exchange and correlation to obtain a range of theoretical values of α which extends down to the measured values.

Further clarification of the relevant dynamic mechanisms operating in the homogeneous electron gas seems useful. To second order in the wave number k the energy-loss spectrum contains contributions from the plasmon and from single-pair as well as multi-pair excitations. For frequencies ω comparable to or larger than the plasma frequency ω_{pl} the main multi-pair contributions arise from two-pair excitations. Starting with the pioneering work of Dubois (see [15, 16]), these have been studied via perturbative methods by several authors [17–23]. The inclusion of dynamic screening leads to a mode-coupling form of the spectrum [18] and a similar expression has been obtained recently by Neilson *et al* [24] within a memory function formalism. A mode-coupling channel involves two plasmons which in turn influence the behaviour of the plasmon excitation. Such two-plasmon effects have recently been found to be important in the description of the energy loss of a charged particle travelling through matter [25].

We present a study which elucidates this effect by calculating selfconsistently the plasmon dispersion coefficient, the coupled modes being estimated within a single-pole approximation (SPA) and selfconsistency being imposed via the compressibility and/or the third-spectral-moment sum rule. We have found it useful to carry out calculations in parallel for fermions and for bosons [26], since in the latter plasma the SPA appears to be less drastic and further help can be found in the use of the sum rules to derive upper bounds. Our SPA results for fermions at low coupling strength also find support in an RPA calculation of the coupled modes.

The main output of our calculations is the whole spectrum of two-pair excitations at order k^2, which in turn yields the dynamic exchange–correlation potential $f_{xc}(\omega)$ for time-dependent density functional theory within the local density and linear response approximations [27]. The result coming for this function from our essentially microscopic approach shows a qualitatively different behaviour from the interpolation formula presented by Gross, Kohn and Iwamoto (see [28–30]). In essence, the two-plasmon coupling mechanism that we have evaluated accumulates oscillator strength in the two-pair spectrum at frequencies in the neighbourhood of $2\omega_{pl}$ and this enforces a highly non-monotonic dependence on frequency for the real part of $f_{xc}(\omega)$. In particular $\mathrm{Re}[f_{xc}(\omega)]$ at frequency ω_{pl} is more strongly attractive than $f_{xc}(0)$.

2. General relations

The density–density response function $\chi(k,\omega)$ is related to the proper polarizability $\Pi(k,\omega)$ by

$$\chi(k,\omega) = \frac{\Pi(k,\omega)}{1 - v_k \Pi(k,\omega)} \tag{2.1}$$

and to the local field factor $G(k, \omega)$ by

$$\chi(k, \omega) = \frac{\chi_0(k, \omega)}{1 - v_k \chi_0(k, \omega)[1 - G(k, \omega)]}. \tag{2.2}$$

Here, $v_k = 4\pi e^2/k^2$ is the Fourier transform of the Coulomb potential and $\chi_0(k, \omega)$ stands for the response function of non-interacting fermions or bosons [6, 31]. The RPA is recovered by setting $G(k, \omega) = 0$ or $\Pi(k, \omega) = \chi_0(k, \omega)$.

Lipparini *et al* [13] have argued that, if Π is decomposed into single-pair (sp) and multi-pair (mp) contributions, $\mathrm{Im}(1/\Pi^{sp})$ coincides with $\mathrm{Im}(1/\chi^0)$ in the long-wavelength limit. Using this, the following relations hold to leading order in k:

$$-\operatorname{Im} G(k \to 0, \omega) \approx \left(1 - \frac{\omega^2}{\omega_{pl}^2}\right)^2 v_k \operatorname{Im} \chi^{mp}(k, \omega) \approx \frac{\omega^4}{\omega_{pl}^4} v_k \operatorname{Im} \Pi^{mp}(k, \omega). \tag{2.3}$$

To the same order the limiting values of the local field factor are known exactly, $G(k, 0)$ from the compressibility sum rule and $G(k, \infty)$ from the third-moment sum rule. They take the form

$$G(k, 0) \simeq \frac{2\varepsilon_k}{\rho \omega_{pl}^2} \left(\frac{1}{K_T^0} - \frac{1}{K_T}\right) \tag{2.4}$$

and

$$G(k, \infty) \simeq -\frac{4\varepsilon_k}{\omega_{pl}^2} \left(\frac{2}{15}\varepsilon_{\mathrm{pot}} + \varepsilon_{\mathrm{kin}} - \varepsilon_{\mathrm{kin}}^0\right) \tag{2.5}$$

where $\varepsilon_k = k^2/2m$, ρ is the density, K_T the isothermal compressibility and $\varepsilon_{\mathrm{pot\ (kin)}}$ the potential (kinetic) energy per particle. The index 0 denotes ideal-gas values. The right-hand sides of equations (2.4) and (2.5) can be evaluated from Monte Carlo data on the ground-state energy and momentum distribution, which are available both for fermions [32, 33] and for bosons [34].

We also recall that the quantity

$$f_{xc}(\omega) = -\lim_{k \to 0} v_k G(k, \omega) \tag{2.6}$$

is the exchange–correlation potential entering time-dependent density functional theory in the local density and linear response approximations [27]. Equations (2.6) and (2.3) show that the imaginary part of $f_{xc}(\omega)$ is directly related to the multi-pair spectrum. A simple formula for $\operatorname{Im} G(k, \omega)$ incorporating low-frequency and high-frequency behaviours, which implies a smooth interpolation between the two limits given in equations (2.4) and (2.5) for $\operatorname{Re} G(k, \omega)$, has been proposed by Gross, Kohn and Iwamoto (see [28–30]).

In the present work the imaginary part of $G(k \to 0, \omega)$ will be evaluated within suitable microscopic approximations and its real part will be derived from it by means of Kramers–Kronig relations [35], namely

$$\operatorname{Re} G(k, \omega) = G(k, \infty) + \frac{1}{\pi} \mathcal{P} \int_{-\infty}^{\infty} \mathrm{d}\omega' \operatorname{Im} G(k, \omega') \frac{1}{\omega' - \omega} \tag{2.7}$$

or alternatively

$$\operatorname{Re} G(k, \omega) = G(k, 0) + \frac{1}{\pi} \mathcal{P} \int_{-\infty}^{\infty} \mathrm{d}\omega' \operatorname{Im} G(k, \omega') \left(\frac{1}{\omega' - \omega} - \frac{1}{\omega'}\right) \tag{2.8}$$

($\mathcal{P}$ denotes the principal value). No *a priori* assumptions will be made on the value of $\mathrm{Re}\, G(k \to 0, \omega_{pl})$, which determines the plasmon dispersion coefficient α via

$$\mathrm{Re}\, G(k \to 0, \omega_{pl}) = (\alpha_{\mathrm{RPA}} - \alpha)\frac{2k^2}{m\omega_{pl}}. \tag{2.9}$$

The dispersion coefficient α_{RPA} in the RPA is zero for bosons and equals $3\varepsilon_F/5\omega_{pl}$ for fermions, ε_F being the Fermi energy.

3. The multi-pair spectrum

In the limit of small k and finite ω Hasegawa and Watabe [18] (HW) derived for the two-pair excitations the result

$$\mathrm{Im}\, G(k,\omega) = \frac{\varepsilon_k}{\pi\rho\omega_p^2}\int_0^\omega \mathrm{d}\omega' \sum_{\boldsymbol{q}} \mathrm{Im}\, v_q \chi(q, \omega-\omega') \times\left[\frac{23}{15}\,\mathrm{Im}\, v_q\chi(q,\omega') + \frac{16}{15}\frac{q^2}{\omega^2}\mathrm{Im}\, v_q\chi_T(q,\omega')\right] \tag{3.1}$$

where the response functions are those of the RPA. The transverse function $\chi_T(k,\omega)$ in the RPA is defined in appendix A (equation (A.11)). There we also discuss in detail the phenomenological inclusion of exchange effects that we have adopted in this work.

Evidently the excitations at frequency ω' are coupled in equation (3.1) with those at frequency $\omega - \omega'$, implying a plasmon–plasmon contribution in parallel with channels involving single-particle excitations and transverse currents. Starting with a positive value of the dispersion coefficient α in the electron fluid at weak coupling, from the structure of equation (3.1) a peak must be expected in $\mathrm{Im}\, G(k \to 0, \omega)$ at around twice the plasma frequency. The oscillator strength there must increase with increasing coupling as the plasmon dispersion curve flattens out and the resonance spreads over a wider region of $\boldsymbol{q}$-space. Thus, as the value of α moves towards zero, an increasingly rapid drop of α is to be expected. The peak may then move towards lower frequencies once α attains negative values.

Before we proceed to an explicit demonstration of such dynamic behaviour via a simple model incorporating the selfconsistency on the value of α which is implied by the argument given above, we remark that the theoretical approach developed recently by Neilson *et al* [24] (NSSS) for the two-dimensional electron gas leads to similar conclusions by an alternative route. While the HW derivation of equation (3.1) was based on the study of the equations of motion for Green's functions, NSSS evaluate the dynamic response on the basis of Mori's memory function formalism. As a first step the single-particle memory function in their result may be neglected, yielding for the imaginary part of the local field factor the expression

$$\mathrm{Im}\, G(k,\omega) = \frac{1}{\pi\rho m\omega_{pl}^2 k^2}\int_0^\omega \mathrm{d}\omega' \sum_{\boldsymbol{q}} \bar{v}_{\boldsymbol{q}}(\boldsymbol{q}\cdot\boldsymbol{k})\,\mathrm{Im}\,\chi(\boldsymbol{q},\omega') \times\mathrm{Im}\,\chi(\boldsymbol{k}-\boldsymbol{q},\omega-\omega')\left[\bar{v}_{\boldsymbol{q}}(\boldsymbol{q}\cdot\boldsymbol{k}) + \bar{v}_{\boldsymbol{k}-\boldsymbol{q}}(k^2 - \boldsymbol{q}\cdot\boldsymbol{k})\right]. \tag{3.2}$$

Here $\bar{v}_k$ is a statically screened potential of the STLS type [2]. The coupled-mode structure of the dynamic local field factor is again evident from equation (3.2), although the transverse response function entering equation (3.1) is missing (see appendix A).

Selfconsistency is built into the calculations that we present immediately below by evaluating the first contribution in equation (3.1) within the SPA,

$$v_k \,\mathrm{Im}\,\chi(k,\omega) = -\frac{\pi\omega_{pl}^2}{2\omega_k}\left[\delta(\omega-\omega_k)-\delta(\omega+\omega_k)\right]. \tag{3.3}$$

Dropping the transverse term in the square brackets in equation (3.1), this equation simplifies to

$$\mathrm{Im}\,G(k,\omega) = \frac{23}{15}\frac{\pi\varepsilon_k}{(2\pi)^3\rho}\int \mathrm{d}^3\boldsymbol{q}\;\delta\big(\omega-2\omega_q\big)\,\frac{\omega_{pl}^2}{\omega^2}. \tag{3.4}$$

Since we are mainly interested in the plasmon dispersion at small k, we transcend the RPA at the same time by adopting for the mode frequency ω_k in equation (3.3) the expression

$$\omega_k = \sqrt{\omega_{pl}^2 + 4\alpha\varepsilon_k\omega_{pl} + \varepsilon_k^2}. \tag{3.5}$$

This interpolates between small- and large-k behaviours while it allows us to keep selfconsistent account of the dispersion coefficient α. We also remark that for the degenerate plasma of bosons a single-mode description of the density response function is the outcome of a vast class of Feynman-like theories [36].

We may also make a clear comparison between the NSSS and the HW results if we replace in equation (3.2) the statically screened potential by the bare potential. Using the SPA we then find in the $k \to 0$ limit

$$\mathrm{Im}\,G(k,\omega) = \frac{7}{15}\frac{\pi\varepsilon_k}{(2\pi)^3\rho}\int \mathrm{d}^3\boldsymbol{q}\;\delta\big(\omega-2\omega_q\big)\,\frac{\omega_{pl}^2}{\omega^2} \tag{3.6}$$

which agrees with the HW expression in equation (3.4) apart from the prefactor. Whereas the HW expression gives the correct perturbational limit derived by Glick and Long [19], the NSSS approach globally includes multi-pair effects to all orders. Neither of the two prefactors seems obviously superior to the other (cf. appendix A).

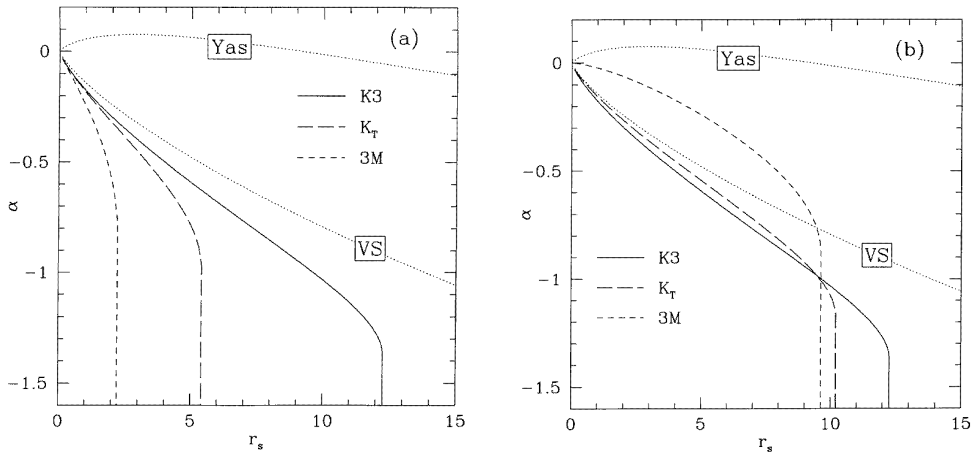

Figure 1. The selfconsistent plasmon dispersion coefficient α for bosons as a function of r_s. (a) HW; (b) NSSS.

4. Plasmon dispersion

In this section we apply the results obtained above to the selfconsistent evaluation of the plasmon dispersion coefficient. Using equation (3.5) in the expressions for the imaginary part of $G(k, \omega)$ given by either equation (3.4) or equation (3.6), the real part of $G(k, \omega)$ can be obtained via one of the two Kramers–Kronig relations given in equation (2.7) or equation (2.8). One may then compute the dispersion coefficient α from equation (2.9) and hence return to a better estimation of the single-mode frequency in equation (3.5). Evidently, we do have a set of equations to be solved selfconsistently, but with possible alternative choices for the strength of the multi-pair spectrum (the prefactor in equations (3.4) and (3.6)) and for the sum rule to be satisfied (equations (2.7) and (2.8)).

Table 1. The plasmon dispersion coefficient α for bosons as a function of r_s, using different models.

r_s	α_{VS}	α_{Yas}	α_{GK}	α_{IG}	α_{K3}
0.1	−0.006 44	0.003 25	—	−0.002 59	−0.007 94
1	−0.0362	0.0140	—	−0.0177	−0.0445
2	−0.0608	0.0182	−0.0608	−0.0335	−0.0746
3	−0.0822	0.0191	−0.0822	−0.0490	−0.1010
4	−0.1018	0.0181	−0.1017	−0.0643	−0.1253
5	−0.1200	0.0159	−0.1199	−0.0793	−0.1483
6	−0.1372	0.0129	−0.1370	−0.0939	−0.1705
10	−0.199	−0.003	−0.198	−0.149	−0.258
12	−0.226	−0.012	−0.225	−0.174	−0.318
15	−0.264	−0.027	−0.263	−0.211	—
20	−0.322	−0.050	−0.320	−0.266	—

We examine below the results given by all these alternatives and also present what we believe to be the best result within our approximate approach. This is obtained by introducing a further parameter β as an overall multiplicative factor for the imaginary part of the local field factor. We are then enabled to carry out a fully selfconsistent evaluation of both α and β by imposing the conditions that both the third-moment sum rule in equation (2.7) and the compressibility sum rule in equation (2.8) must be exactly satisfied.

Table 2. The plasmon dispersion coefficient α for fermions as a function of r_s, using different models.

r_s	α_{VS}	α_{Yas}	α_{GK}	α_{IG}	α_{K3}
0.1	1.998 68	2.007 37	2.000 71	2.001 80	1.998 16
1	0.5768	0.6164	0.5791	0.5884	0.5731
2	0.362	0.426	0.364	0.380	0.355
3	0.256	0.340	0.259	0.279	0.246
4	0.187	0.288	0.189	0.214	0.174
5	0.135	0.252	0.137	0.165	0.119
6	0.093	0.223	0.096	0.125	0.074
10	−0.026	0.150	−0.023	0.014	−0.057
12	−0.070	0.124	−0.067	−0.028	−0.108
15	−0.127	0.092	−0.123	−0.082	−0.179
20	−0.206	0.049	−0.201	−0.157	−0.320

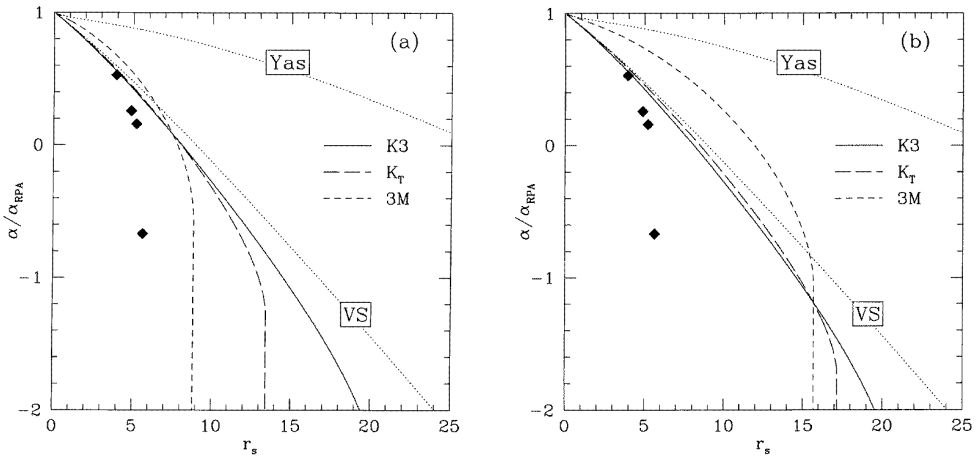

Figure 2. The selfconsistent plasmon dispersion coefficient $\alpha/\alpha_{\rm RPA}$ for fermions as a function of r_s. Also included are the experimental results obtained by vom Felde *et al* [1] (lozenges). (a) HW; (b) NSSS.

The results for the plasmon dispersion coefficient α at selfconsistency are shown in tables 1 and 2 and in figures 1 and 2. The notation used in these figures is as follows:

(i) K_T denotes a calculation in which α is determined with either the HW or the NSSS choice for the prefactor by satisfying the compressibility sum rule (2.8), thus attributing greater relevance to the low-frequency part of the spectrum;

(ii) $3M$ denotes a calculation in which α is determined with either the HW or the NSSS choice for the prefactor by satisfying the third-moment sum rule (2.7), thus attributing greater relevance to the high-frequency part of the spectrum;

(iii) $K3$ denotes a calculation in which α and β are determined by satisfying both sum rules. Evidently, the difference between HW and NSSS results disappears. In the relevant density range ($r_s \sim$ 2–15) we find that β/β_{HW} is a decreasing function ranging from 2 to 0.5.

Our results in figures 1 and 2 are also compared with those obtained by neglecting the imaginary part of the local field factor (i.e. taking $\beta = 0$) and setting $G(k, \omega_{pl})$ equal either to $G(k, 0)$ or to $G(k, \infty)$. The former was done by Vashishta and Singwi [3] and yields an upper bound on both K_T and $K3$. The latter was done by Suehiro *et al* [37] and yields an upper bound on both $3M$ and $K3$. We use the notation VS and Yas for the corresponding results both for bosons and for fermions, as obtained from the Monte Carlo equation of state. Tables 1 and 2 report these numerical values for the dispersion coefficient at various values of r_s, together with those computed from the Gross–Kohn (GK) and the Iwamoto–Gross (IG) local field correction and with those that we obtain in our 'best' selfconsistent calculation (indicated as α_{K3}). Of course, the GK and IG values lie between the Yas and the VS results. The limited accuracy of the fits to Monte Carlo data involved in these evaluations [34, 38] is likely to affect the last significant figure in the numerical values of α reported in these tables.

Figure 1 shows the behaviour of α as a function of r_s for bosons. In all approaches except the Yas one, α is negative throughout the whole density range. It has recently been shown from sum rule arguments that the VS result provides an exact upper bound on the plasmon dispersion coefficient in the degenerate plasma of bosons [39]. Our best result,

given by the full curve in figure 1, correctly lies below this upper bound. The steep drop of α at $r_s \sim 12$ is due to a breakdown of the SPA as we discuss below in the case of fermions.

Figure 2 reports the behaviour of $\alpha/\alpha_{\mathrm{RPA}}$ as a function of r_s for fermions. All our results show a rapidly increasing drop in the plasmon dispersion coefficient with increasing r_s and again our best result lies below the VS result at all values of r_s. This behaviour arises from the mutual repulsion between the single-plasmon excitation and the two-pair excitations, with the spectrum of the latter starting within the SPA at twice the minimum frequency ω_{min} in the single-mode dispersion curve. This repulsion increases with decreasing energy difference (i.e. at smaller α) and with increasing oscillator strength in the low-frequency part of the two-pair spectrum (again at smaller α). Therefore, the selfconsistent iterations in α lead to a rapid softening of the plasmon as is seen in figure 2. Evidently the SPA breaks down at a density such that ω_{min} reaches $\omega_{pl}/2$, where the decay of a plasmon into two modes at $\boldsymbol{k}_{min}$ and $-\boldsymbol{k}_{min}$ would become possible.

Finally, figure 2 also reports the measured values of $\alpha/\alpha_{\mathrm{RPA}}$ in the four alkali metals from Na to Cs [1]. It is clear that the plasmon softening mechanism that we have evaluated is still insufficient to account for these observations by itself.

5. The dynamic exchange–correlation potential for fermions

Having obtained a selfconsistent solution for α we are now able to discuss the frequency dependence of the local field factor at long wavelength, i.e. of the exchange–correlation potential $f_{xc}(\omega)$ defined in equation (2.6). We shall do this with the main attention focused on fermions in the $K3$ approach, which is fully consistent and ensures the correct limiting behaviours of Re $f_{xc}(\omega)$ at both high and low frequency according to equations (2.7) and (2.8).

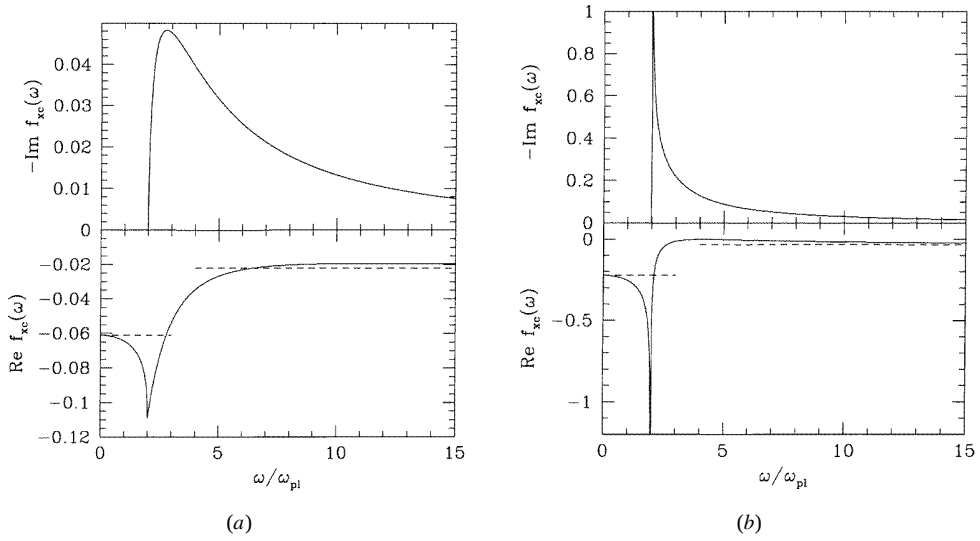

Figure 3. Real and imaginary parts of $f_{xc}(k,\omega)$ at small k in units of $2\omega_{pl}/\rho$, as functions of ω/ω_{pl} from the SPA for fermions at $r_s = 1$ (a) and $r_s = 10$ (b). The asymptotic behaviours are shown by the dashed lines.

It is easily seen that Im $f_{xc}(\omega)$ decreases as $\omega^{-3/2}$ for large ω. As a consequence of the SPA it vanishes at frequencies below $2\omega_{min}$. For positive α a continuous function with an

infinite right-hand-side derivative at $2\omega_{min}$ is obtained (figure 3(a)), whereas for negative α a divergence of the type $(\omega - 2\omega_{min})^{-1/2}$ is found (figure 3(b)). This in turn leads to a cusp in Re $f_{xc}(\omega)$ for positive α and to a singularity of the type $(2\omega_{min} - \omega)^{-1/2}\,\theta(2\omega_{min} - \omega)$ if α is negative (figure 3). In all cases Re $f_{xc}(k, \omega)$ at low frequency lies below the value $f_{xc}(0)$ given by the compressibility sum rule and the limiting value $f_{xc}(\infty)$ corresponding to the third moment is reached from above. While the above-mentioned singularities at $2\omega_{min}$ are consequences of the SPA, singularities in the two-pair spectrum at $2\omega_{pl}$ arise even in the RPA (see below).

The behaviour of $f_{xc}(\omega)$ shown in figure 3 is qualitatively different from the results of Gross, Kohn and Iwamoto (see [28–30]), who proposed a smooth and essentially monotonic interpolation between the static and the high-frequency limits. The question arises of whether or not the pronounced structure that we find in the frequency dependence of Re $f_{xc}(\omega)$ is an artifact of our model and in particular of the SPA.

As we have recalled in section 4, in the case of bosons an upper bound on the plasmon dispersion coefficient has been demonstrated from an exact sum rule argument [39] and it coincides with the VS result. Consequently Re $f_{xc}(\omega_{pl})$ must lie below $f_{xc}(0)$, implying the presence of a minimum at finite ω since $f_{xc}(\infty)$ lies above $f_{xc}(0)$. A structure in the frequency dependence of Re $f_{xc}(\omega)$ of the type that we have found is thus correct for the boson plasma at all couplings.

No such exact statement can be made at present for fermions. An independent, though still approximate assessment of the quality of the SPA results can be made at weak coupling by evaluating $f_{xc}(\omega)$ from the original HW formula in equation (3.1), using the RPA expressions for the linear response functions appearing there.

5.1. The RPA calculation of the exchange–correlation potential

We have already seen from equation (3.1) that $f_{xc}(\omega)$ involves a density–density (dd) contribution and a density–transverse-current (dt) contribution. We focus first on the dd term and shall later evaluate the dt term. For a meaningful quantitative comparison with the SPA and IG/GK results we shall rescale the final RPA and SPA curves so as to ensure consistency with both the compressibility and the third-moment sum rule. For the same reason the SPA curves use the RPA value of the dispersion coefficient α, rather that the selfconsistent one.

From the RPA expression for the density response function $\chi(k, \omega)$, the dd term involves plasmon–plasmon (pp), plasmon–continuum (pc) and continuum–continuum (cc) components. Figure 4(a) reports these three separate components as evaluated at $r_s = 1$, as well as their sum (full curve) yielding the dd contribution to the imaginary part of $f_{xc}(\omega)$. The individual components show singularities at ω_c and $2\omega_c$, ω_c being the frequency where the plasmon dispersion curve crosses the edge of the single-pair continuum. However, these singularities cancel away in the sum. On the other hand, the singularities at ω_{pl} and $2\omega_{pl}$ arise from real phase-space effects and are present in the components as well as in their sum. Appendix B gives an analytic treatment of the singularity which is brought by the pp spectral component into the real part of the exchange–correlation potential at $2\omega_{pl}$.

The above RPA result for the two-pair spectrum is compared with the SPA result in figure 4(b). The main difference is that, while the SPA spectrum vanishes at frequencies below $2\omega_{pl}$, the cc and pc components of the RPA spectrum do not. However, their spectral weight is quite small in this frequency range, since the cc and pc two-pair excitations involve single-pair excitations and these have low oscillator strength at low frequencies. This fact is explicitly illustrated in figure 5, reporting the momentum-integrated oscillator strength of

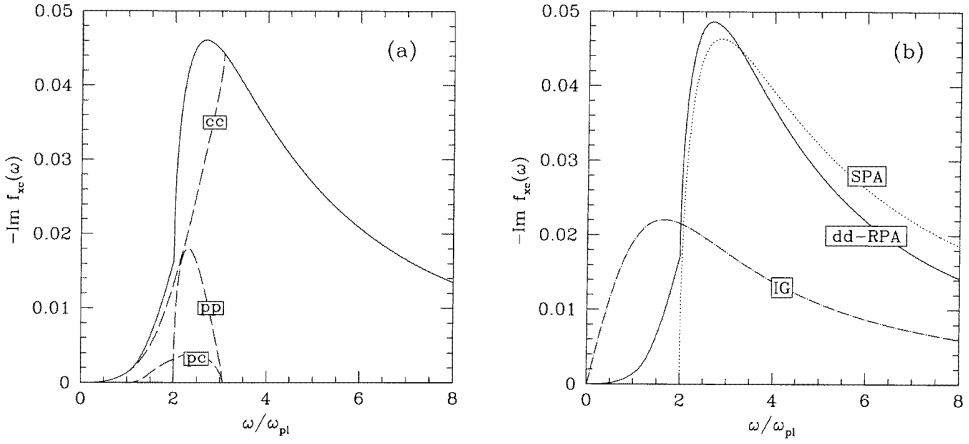

Figure 4. The imaginary part of $f_{xc}(\omega)$, in units of $2\omega_{pl}/\rho$, as a function of ω/ω_{pl} at $r_s = 1$. (a) The dd spectrum (full curve) and its components in the RPA; (b) the dd spectrum in the RPA compared with the SPA and IG spectra, after rescaling to satisfy the compressibility and third-moment sum rules.

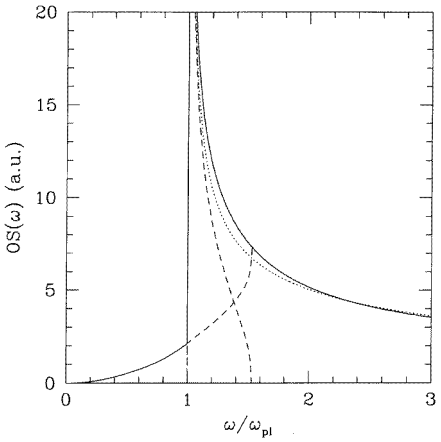

Figure 5. The momentum-integrated oscillator strength at $r_s = 1$ as a function of ω/ω_{pl} in the RPA (full curve) and SPA (dotted curve). The two dashed curves give the plasmon and continuum contributions to the RPA result.

the density-fluctuation spectrum,

$$\mathrm{OS}(\omega) = \int \mathrm{d}^3\boldsymbol{k}\ \omega v_k \,\mathrm{Im}\,\chi(k,\omega) \tag{5.1}$$

in the RPA and in the SPA at $r_s = 1$. Figure 4(b) also reports the IG result for the two-pair spectrum, showing that it places a large part of the spectral weight at low frequencies.

After Kramers–Kronig transform the results in figure 4 yield the dd contribution to the real part of $f_{xc}(\omega)$ as reported in figure 6. The full RPA curve exhibits a sharp spike at $2\omega_{pl}$, just as the SPA does (see appendix B). Owing to the presence of oscillator strength for two-pair excitations below $2\omega_{pl}$ in the RPA calculation, its value for the plasmon dispersion coefficient is somewhat smaller than in the SPA if the same input α is used. It is also evident

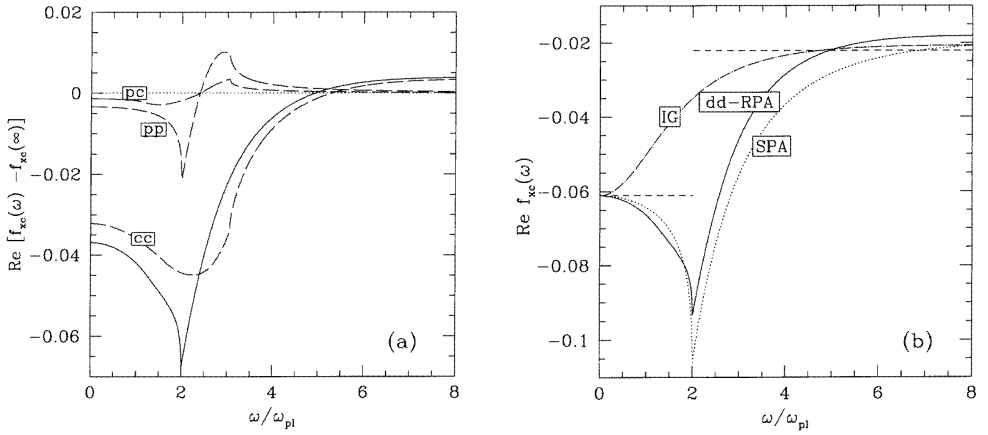

Figure 6. The real part of $f_{xc}(\omega)$, in units of $2\omega_{pl}/\rho$, as a function of ω/ω_{pl} at $r_s = 1$. (a) The dd result (full curve) and its components in the RPA; (b) the dd result in the RPA compared with the SPA and IG results, after rescaling to satisfy the compressibility and third-moment sum rules.

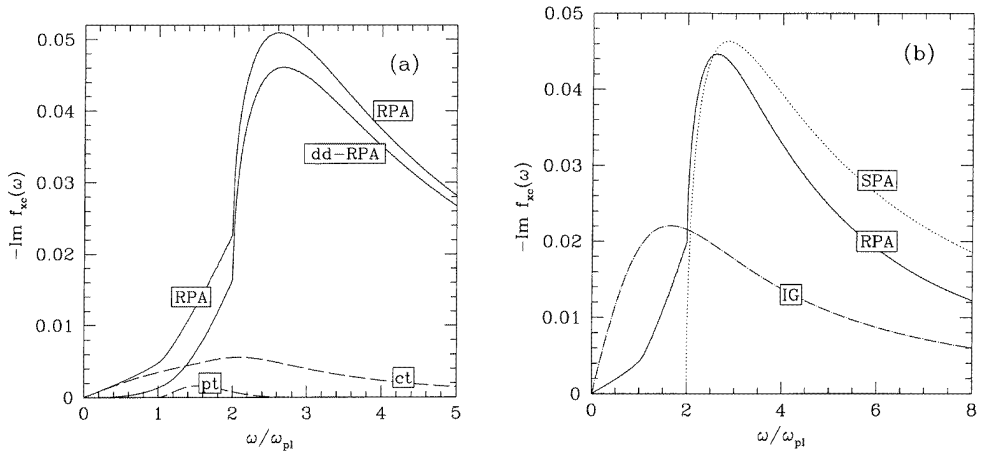

Figure 7. The imaginary part of $f_{xc}(\omega)$, in units of $2\omega_{pl}/\rho$, as a function of ω/ω_{pl} at $r_s = 1$. (a) The contributions to the RPA spectrum; (b) the RPA spectrum compared with the SPA and IG spectra, after rescaling to satisfy the compressibility and third-moment sum rules.

from figure 6(b) that the IG result has an entirely different dependence on frequency in the intermediate region between the same low- and high-frequency limits. While the results of an RPA calculation can be relied upon only at low coupling strength, calculations that we have carried out at $r_s = 10$ yield conclusions similar to those emerging from figures 4 and 6. Of course, the pp channel becomes relatively more important with increasing coupling strength.

We finally turn to an RPA evaluation of the dt contribution to $f_{xc}(\omega)$. When retardation is neglected ($c \to \infty$) the transverse response function entering equation (3.1) reduces in the RPA to the transverse response function of the ideal Fermi gas [40]. Explicit expressions for the latter are given in appendix C. On inserting these in equation (3.1) it is evident

that the dt contribution involves two components, i.e. (i) a ct component arising from a single-pair density excitation and a single-pair transverse excitation and (ii) a pt component arising from a plasmon and a single-pair transverse excitation. Figure 7(a) reports these components of the two-pair spectrum at $r_s = 1$ and compares the total result for the two-pair spectrum in the RPA (the full curve labelled RPA) with the result obtained in figure 4(a) for the dd channel. The total RPA result is compared with the SPA result and with the IG result in figure 7(b). The corresponding results for the real part of the exchange–correlation potential are shown in figure 8.

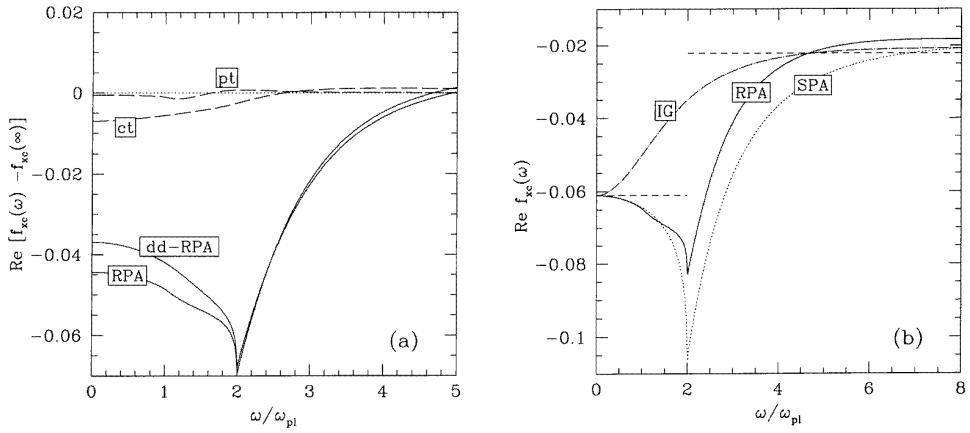

Figure 8. The real part of $f_{xc}(\omega)$, in units of $2\omega_{pl}/\rho$, as a function of ω/ω_{pl} at $r_s = 1$. (a) The contributions to the RPA results; (b) the RPA result compared with the SPA and IG results, after rescaling to satisfy the compressibility and third-moment sum rules.

The main consequences of including the dt channel in the two-pair spectrum arise in the low-frequency region. In particular, in the limit $\omega \to 0$ the dt component of the RPA two-pair spectrum is linear in ω, just as the IG result is, though with a very different slope (see figure 7(b)). In the same limit the dd component is instead proportional to ω^3, the difference by a factor ω^2 being evident e.g. from equation (A.8). The oscillator strength residing in the transverse excitations at low frequency induces through the pt component some structure in Re $f_{xc}(\omega)$ in the region of the plasma frequency, as can be seen from figure 8.

6. Concluding remarks

In summary, we have presented a selfconsistent model to describe the effects of two-pair excitations on plasmon dispersion and on the shape of the dynamic local field factor for exchange and correlation at small wave number. A pronounced structure is found in the frequency dependence of the real part of the local field factor, even at small values of r_s where the plasmon dispersion coefficient is still positive. In the region of coupling strength where the single-mode approximation made in our calculations can be expected to be reasonably close to correctness, our results for the selfconsistently determined dispersion coefficient show rapid softening of the plasmon excitation. Since the real part of the exchange–correlation potential is more strongly attractive at the plasma frequency than at zero frequency, future inclusion of band-structure effects for alkali metals by means of

time-dependent density functional theory may we hope provide a fully satisfactory account of the existing observations.

Appendix A. Multi-pair excitations to lowest order

The two-pair contribution to the imaginary part of the proper polarizability of fermions was first derived by diagrammatic means by Glick and Long [19] to lowest order in the interaction v_k. Introducing the function

$$\begin{aligned} X(\boldsymbol{q},\boldsymbol{p},\boldsymbol{p}',\boldsymbol{k}) &= \theta(k_F-p)\,\theta(|\boldsymbol{p}+\boldsymbol{k}-\boldsymbol{q}|-k_F)\theta(k_F-p')\,\theta(|\boldsymbol{p}'+\boldsymbol{q}|-k_F) \\ &\quad\times\delta\Big(m\omega+(\boldsymbol{p}-\boldsymbol{p}')\cdot\boldsymbol{q}+(\boldsymbol{q}-\boldsymbol{p})\cdot\boldsymbol{k}-\tfrac{1}{2}k^2-q^2\Big) \end{aligned} \tag{A.1}$$

with k_F the Fermi momentum, their result can be cast into the form

$$\begin{aligned} \operatorname{Im}\Pi^{2P0}(k,\omega) &= -\frac{\pi m^3}{2}\sum_{\sigma,\sigma'}\sum_{\boldsymbol{q},\boldsymbol{p},\boldsymbol{p}'}X(\boldsymbol{q},\boldsymbol{p},\boldsymbol{p}',\boldsymbol{k})\Big[A(\boldsymbol{q},\boldsymbol{p},\boldsymbol{k})+A(\boldsymbol{k}-\boldsymbol{q},\boldsymbol{p}',\boldsymbol{k})\Big] \\ &\quad\times\Big\{\Big[A(\boldsymbol{q},\boldsymbol{p},\boldsymbol{k})+A(\boldsymbol{k}-\boldsymbol{q},\boldsymbol{p}',\boldsymbol{k})\Big]-\delta_{\sigma,\sigma'}\Big[\ldots(\text{exch})\ldots\Big]\Big\}. \end{aligned} \tag{A.2}$$

Here, the function A is defined as

$$A(\boldsymbol{q},\boldsymbol{p},\boldsymbol{k})=\frac{v_q\,\boldsymbol{q}\cdot\boldsymbol{k}}{\Big[m\omega-(\boldsymbol{p}+\frac{1}{2}\boldsymbol{k})\cdot\boldsymbol{k}\Big]\Big[m\omega-(\boldsymbol{p}-\frac{1}{2}(\boldsymbol{k}+\boldsymbol{q}))\cdot\boldsymbol{k}\Big]}. \tag{A.3}$$

Obviously the terms headed by $\delta_{\sigma,\sigma'}$ describe exchange effects. Their explicit form is not required here, since they can be accounted for by physical arguments (cf. below). It is further to be noticed that the symmetry of the integrand in equation (A.2) allows the replacement of the first bracket by $2A(\boldsymbol{q},\boldsymbol{p},\boldsymbol{k})$.

Equation (A.2) is valid for arbitrary values of (k,ω) outside the particle–hole continuum. In the limit of high frequency and finite wave vector the restriction of $\boldsymbol{p}$ and $\boldsymbol{p}'$ to the Fermi sphere implies that

$$X(\boldsymbol{q},\boldsymbol{p},\boldsymbol{p}',\boldsymbol{k})\approx\theta(k_F-p)\theta(k_F-p')\,\delta\Big(m\omega-q^2\Big) \tag{A.4}$$

and

$$A(\boldsymbol{q},\boldsymbol{p},\boldsymbol{k})\approx\frac{v_q\,\boldsymbol{q}\cdot\boldsymbol{k}}{(m\omega)^2}\left[1-\frac{\boldsymbol{q}\cdot\boldsymbol{k}}{m\omega}+\ldots\right]. \tag{A.5}$$

From these relations it follows [19] that

$$v_k\operatorname{Im}\Pi(k,\omega\to\infty)=-\frac{23\pi}{80}\left(\frac{k}{k_F}\right)^2\frac{(\omega_{\mathrm{pl}}/2\varepsilon_F)^6}{(\omega/2\varepsilon_F)^{11/2}}. \tag{A.6}$$

The contribution to equation (A.6) due to exchange cancels one half of the direct result. This can be understood in the following way. Although the Fermi functions in X ensure that excitations only occur from occupied to empty states, they do not enforce different spins for particles having equal momenta. This case arises for energy transfers which are large in comparison with the Fermi energy ε_F and reduces the allowed phase space by a factor 1/2. In the opposite limit of small ω, excitations take place on the Fermi surface. Here, the processes involving identical final momenta are a vanishing fraction of all possible transitions and the function X correctly describes the available phase space.

The main effect of the exchange contributions thus is to modify X by a factor ranging from 1 to $\frac{1}{2}$ for frequencies ranging from $\omega \ll \varepsilon_F$ to $\omega \gg \varepsilon_F$. This can be conveniently accounted for by introducing a simple function $f(\omega)$, whose specific form is found to have only a minor influence on the results. We suggest using

$$f(\omega) = \frac{1 + (\omega/2\varepsilon_F) + 0.5(\omega/2\varepsilon_F)^2}{1 + (\omega/2\varepsilon_F) + (\omega/2\varepsilon_F)^2}. \tag{A.7}$$

This function is understood to be included, together with the usual V^{-1}, in the $\boldsymbol{q}$-summation for fermions in both the following equations of this appendix and in equations (3.1)–(3.4) and (3.6) in the main text, without being explicitly written.

If equation (A.2) is expanded to lowest order in $\boldsymbol{k}$ (i.e. for $k^2 \ll m\omega$) one obtains the result [21]

$$\operatorname{Im} v_k \, \Pi^{2P0}(k \to 0, \omega) = -\frac{\pi}{2} \frac{k^2 \omega_{\mathrm{pl}}^2}{\rho \omega^4} \sum_{\boldsymbol{q},\boldsymbol{p},\boldsymbol{p}'} X(\boldsymbol{q}, \boldsymbol{p}, \boldsymbol{p}', 0) v_q^2 \left\{ \frac{23}{15} + \frac{16}{15} \left(\frac{q \; p_T}{m \, \omega} \right)^2 \right\} \tag{A.8}$$

where p_T denotes a transverse component of the wave vector ($p^2 = 2p_T^2 + (\boldsymbol{p} \cdot \boldsymbol{q}/q)^2$). Equation (A.8) was originally derived by Hasegawa and Watabe [18] using Green's function methods. In addition they suggested including dynamic screening by decoupling the highest-order propagator into the product of pair propagators, leading to the result given in equation (3.1) of the main text. Noting that

$$\frac{\pi}{2} \, X(\boldsymbol{q}, \boldsymbol{p}, \boldsymbol{p}', \boldsymbol{k}) = \int_0^\omega \frac{\mathrm{d}\omega'}{2\pi} \operatorname{Im} \chi_{\boldsymbol{p}}^0(\boldsymbol{k} - \boldsymbol{q}, \omega - \omega') \operatorname{Im} \chi_{\boldsymbol{p}'}^0(\boldsymbol{q}, \omega') \tag{A.9}$$

in terms of elementary ideal-gas processes of single-particle excitation, one can immediately identify the second term in the brackets in equation (A.8) as arising from the transverse free response function. This is related to the RPA transverse dielectric function [40] via

$$\epsilon_T^{\mathrm{RPA}}(k, \omega) = 1 - \frac{4\pi e^2}{\omega^2} \left[\chi_T^0(k, \omega) + \frac{\rho}{m} \right] \tag{A.10}$$

with

$$\chi_T^0(k, \omega) = \sum_{\boldsymbol{p},\sigma} \frac{p_T^2}{m^2} \chi_{\boldsymbol{p},\sigma}^0(k, \omega). \tag{A.11}$$

This term does not contribute to the high-frequency limit, as is obvious from equation (A.8).

Finally, we remark that approximating the function A in equation (A.2) by its high-frequency form given in equation (A.5) and additionally neglecting the $\boldsymbol{q} \cdot \boldsymbol{k}/m\omega$ term leads to

$$\begin{aligned} &\operatorname{Im} v_k \Pi^{2P0}(k, \omega) \\ &\quad \approx -\frac{\omega_{\mathrm{pl}}^2}{\rho m \omega^4 k^2} \int_0^\omega \frac{\mathrm{d}\omega'}{\pi} \sum_{\boldsymbol{q}} \operatorname{Im} \chi_0(\boldsymbol{k} - \boldsymbol{q}, \omega - \omega') \operatorname{Im} \chi_0(\boldsymbol{q}, \omega') \\ &\qquad \times v_q \, (\boldsymbol{q} \cdot \boldsymbol{k}) \Big[v_q \, (\boldsymbol{q} \cdot \boldsymbol{k}) + v_{\boldsymbol{k}-\boldsymbol{q}} \, (k^2 - \boldsymbol{q} \cdot \boldsymbol{k}) \Big]. \end{aligned} \tag{A.12}$$

This expression has the form proposed by Neilson *et al* [24], the absence of transverse contributions being consistent with the large-ω assumption. On the other hand, as remarked in section 5.1 the low-frequency behaviour is dominated by the transverse contribution.

For small wave number, equation (A.12) leads to replacing the prefactor 23/80 in equation (A.6) by the value 7/80. Thus the correct lowest-order result is not reproduced

by the NSSS. However, it is not *a priori* obvious that higher-order multi-pair excitations should not affect this factor. Therefore, such a modification of the Glick–Long limit, which still preserves the correct functional dependence of the type $k^2/\omega^{-11/2}$, seems acceptable.

Appendix B. The singularity in Re $f_{xc}(\omega)$ at $2\omega_{pl}$

In this appendix the non-smooth (non-C^1) terms in Re $f_{xc}(\omega)$ around $2\omega_{pl}$ are evaluated analytically in the case where $\alpha > 0$. It is also verified that the result agrees with the numerical evaluation reported in the main text. In the case where $\alpha < 0$ a behaviour of the type $(\omega - \omega_{pl})^{-1/2}$ is easily derived as pointed out in section 5.

The non-smooth contribution to Im $f_{xc}(\omega)$ due to the two-plasmon channel is

$$\text{Im } f_{xc}(\omega \sim 2\omega_{pl}) \propto \theta(\omega - 2\omega_{pl})\sqrt{\omega - 2\omega_{pl}} \tag{B.1}$$

apart from an overall negative constant factor. The real part is obtained by Kramers–Kronig transformation:

$$\text{Re}\left[f_{xc}(\omega) - f_{xc}(\infty)\right] = \int \frac{\mathrm{d}\omega'}{\pi}\ \frac{\text{Im } f_{xc}(\omega')}{\omega' - \omega}. \tag{B.2}$$

The only singular contributions arise for $\omega' = 2\omega_{pl}$, so neglecting smooth terms the integration range can be limited to $[2\omega_{pl}, 2\omega_{pl} + \Delta]$. By making the changes of variable $\omega' = 2\omega_{pl} + x$ and $\omega = 2\omega_{pl} + y$ the integral can be put into the form

$$\int_{2\omega_{pl}}^{2\omega_{pl}+\Delta} \mathrm{d}\omega'\ \frac{\sqrt{\omega' - 2\omega_{pl}}}{\omega' - \omega} = \int_0^{\Delta} \mathrm{d}x\ \frac{x^{1/2}}{x - y}. \tag{B.3}$$

To obtain the non-smooth contributions the above integral has to be evaluated for both positive and negative y.

If $y > 0$, i.e. for $\omega > 2\omega_{pl}$, we have

$$\int_0^{\Delta} \frac{x^{1/2}}{x - y}\ \mathrm{d}x = 2\Delta^{1/2} - y^{1/2}\ \ln\left|\frac{y^{1/2} + \Delta^{1/2}}{y^{1/2} - \Delta^{1/2}}\right| \simeq 2\Delta^{1/2} - \frac{2}{\Delta^{1/2}}y \tag{B.4}$$

while if $y < 0$, i.e. for $\omega < 2\omega_{pl}$ we have

$$\int_0^{\Delta} \frac{x^{1/2}}{x - y}\ \mathrm{d}x = 2\Delta^{1/2} - 2|y|^{1/2}\tan^{-1}\left(\frac{\Delta^{1/2}}{y^{1/2}}\right) \simeq 2\Delta^{1/2} - \pi|y|^{1/2} - \frac{2}{\Delta^{1/2}}y. \tag{B.5}$$

We thus conclude that a singular term is present only on the left of the singularity and is proportional to $-\theta(2\omega_{pl} - \omega)\sqrt{2\omega_{pl} - \omega}$.

Recovering the multiplicative constant this result can also be put in the form

$$\text{Re } f_{xc}(2\omega_{pl} - \delta) = -\text{Im } f_{xc}(2\omega_{pl} + \delta) + \text{smooth function (class } C^1). \tag{B.6}$$

This is compared in figure A1 with the result of the numerical evaluation of Re $f_{xc}(\omega)$ within the SPA, the smooth function being represented by a straight line fitted to the numerical result at $\omega > 2\omega_{pl}$.

Appendix C. The transverse response function of the ideal Fermi gas

The transverse equivalent of the Lindhard response function is given by

$$\text{Im } \chi_T^0(k, \omega) = \pi \int_{\mathcal{F}} \frac{\mathrm{d}^3q}{(2\pi)^3}\ \frac{q_T^2}{m^2}\ \left[\delta\left(\omega - \frac{(\boldsymbol{k} + \boldsymbol{q})^2}{2m} + \frac{q^2}{2m}\right) - \delta\left(\omega + \frac{(\boldsymbol{k} + \boldsymbol{q})^2}{2m} - \frac{q^2}{2m}\right)\right] \tag{C.1}$$

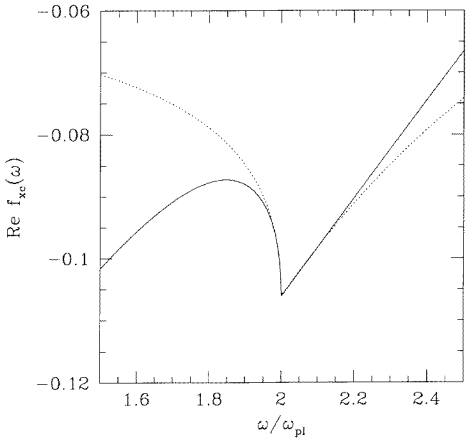

Figure A1. Re $f_{xc}(\omega)$ as obtained numerically around $2\omega_{pl}$ at $r_s = 1$ in the SPA (dotted curve), compared with the singular behaviour given in equation (B.6) added to a straight line (full curve).

where the integration domain $\mathcal{F}$ is the Fermi sphere [40]. By performing the integration we get

$$\operatorname{Im}\chi_T^0(k,\omega) = -\frac{\omega}{16\pi k^3}\left(4k^2{k_F}^2 - k^4 - 4m^2\omega^2\right) \tag{C.2}$$

for $0 < \omega < (2kk_F - k^2)/2m$ and

$$\operatorname{Im}\chi_T^0(k,\omega) = -\frac{1}{256\pi mk^5}\left(k^4 - 4k^2k_F^2 - 4k^2m\omega + 4m^2\omega^2\right)^2 \tag{C.3}$$

for $|2kk_F - k^2|/2m < \omega < (2kk_F + k^2)/2m$. The imaginary part of the transverse response function is zero elsewhere.

The Kramers–Kronig transform of the result in equations (C.2) and (C.3) yields

$$\begin{aligned}\operatorname{Re}\chi_T^0(k,\omega) = {} & \frac{k_F}{96\pi^2mk^2}\left(3k^4 - 20k^2{k_F}^2 + 36m^2\omega^2\right) + \\ & + \frac{1}{256\pi^2mk^5}\left(k^4 - 4k^2{k_F}^2 + 4k^2m\omega + 4m^2\omega^2\right)^2 \ln\left|\frac{\omega + k^2/2m - kk_F/m}{\omega + k^2/2m + kk_F/m}\right| \\ & + \frac{1}{256\pi^2mk^5}\left(k^4 - 4k^2k_F^2 - 4k^2m\omega + 4m^2\omega^2\right)^2 \ln\left|\frac{\omega - k^2/2m + kk_F/m}{\omega - k^2/2m - kk_F/m}\right|.\end{aligned} \tag{C.4}$$

References

[1] vom Felde A, Sprösser-Prou J and Fink J 1989 *Phys. Rev.* B **40** 10 181
[2] Singwi K S, Tosi M P, Land R H and Sjölander A 1968 *Phys. Rev.* **176** 598
[3] Vashishta P and Singwi K S 1972 *Phys. Rev.* B **6** 875
[4] Pathak K N and Vashishta P 1973 *Phys. Rev.* B **7** 3649
[5] Utsumi K and Ichimaru S 1982 *Phys. Rev.* A **26** 603
[6] Singwi K S and Tosi M P 1981 *Solid State Physics* vol 36 (New York: Academic) p 177
[7] Ichimaru S 1982 *Rev. Mod. Phys.* **54** 1017
[8] Parish J L 1990 *Phys. Rev.* B **42** 10 940
[9] Serra L, Garcias F, Barranco M, Barberan N and Navarro J 1991 *Phys. Rev.* B **44** 1492

[10] Ignatchenko V A and Mankov Y I 1991 *J. Phys.: Condens. Matter* **3** 5837
[11] Kalman G, Kempa K and Minella M 1991 *Phys. Rev.* B **43** 14 238
[12] Taut M and Sturm K 1992 *Solid State Commun.* **82** 295
[13] Lipparini E, Stringari S and Takayanagi K 1994 *J. Phys.: Condens. Matter* **6** 2025
[14] Aryasetiawan F and Karlsson K 1994 *Phys. Rev. Lett.* **73** 1679
[15] DuBois D F 1959 *Ann. Phys., NY* **8** 24
[16] DuBois D F and Kivelson M G 1969 *Phys. Rev.* B **186** 409
[17] Ninham B W, Powell C J and Swanson N 1966 *Phys. Rev.* **145** 209
[18] Hasegawa M and Watabe M 1969 *J. Phys. Soc. Japan* **27** 1393
[19] Glick A J and Long W F 1971 *Phys. Rev.* B **4** 3455
[20] Gasser W 1984 *Z. Phys.* B **57** 15
[21] Bachlechner M E, Macke W, Miesenböck H M and Schinner A 1991 *Physica* B **168** 104
[22] Gasser W 1992 *Physica* B **183** 217
[23] Bachlechner M E, Böhm H M and Schinner A 1993 *Phys. Lett.* **178A** 186
[24] Neilson D, Swierkowski L, Sjölander A and Szymanski J 1991 *Phys. Rev.* B **44** 6291
[25] Pitarke J M and Ritchie R H 1994 *Nucl. Instrum. Methods* B **90** 358
[26] We still use the expression 'multi-pair' instead of 'multi-particle' excitations for the degenerate plasma of bosons, with the understanding that the holes are left in the condensate.
[27] Gross E K U and Kohn W 1990 *Adv. Quant. Chem.* **21** 255
[28] Gross E K U and Kohn W 1985 *Phys. Rev. Lett.* **55** 2850
[29] Gross E K U and Kohn W 1986 *Phys. Rev. Lett.* **57** 923
[30] Iwamoto N and Gross E K U 1987 *Phys. Rev.* B **35** 3003
[31] Caparica A and Hipólito O 1982 *Phys. Rev.* A **26** 2832
[32] Ceperley D M and Alder B J 1980 *Phys. Rev. Lett.* **45** 566
[33] Ortiz G and Ballone P 1994 *Phys. Rev.* B **50** 1391
[34] Moroni S, Conti S and Tosi M P 1996 *Phys. Rev.* B to appear
[35] Kugler A A 1975 *J. Stat. Phys.* **12** 37
[36] Conti S, Chiofalo M L and Tosi M P 1994 *J. Phys.: Condens. Matter* **6** 8795
[37] Suehiro H, Ousaka Y and Yasuhara H 1985 *J. Phys. C: Solid State Phys.* **18** 6007
[38] Vosko S H, Wilk L and Nusair M 1980 *Can. J. Phys.* **58** 1200
[39] Chiofalo M L, Conti S, Stringari S and Tosi M P 1995 *J. Phys.: Condens. Matter* **7** L85
[40] Pines D and Nozières P 1966 *The Theory of Quantum Liquids* vol 1 (New York: Benjamin)